https://dx.doi.org/10.1016/j.combustflame.2023.112742

From electronic structure to model application of key reactions for gasoline/alcohol combustion: hydrogen-atom abstractions by CH3Ȯ radical

Kiran K. Yalamanchi[a], Xin Bai[b], Nivain Devnith Fernando[c], Adrian Shalom Lua[c], Song Cheng[c,d,*], Yang Li[b,*], Chong-Wen Zhou[e], S. Scott Goldsborough[d], S. Mani Sarathy[a]

[a]*King Abdullah University of Science and Technology (KAUST), Clean Combustion Research Center, Physical Sciences and Engineering Division, Thuwal, Saudi Arabia*

[b]*Science and Technology on Combustion, Internal Flow and Thermostructure Laboratory, School of Astronautics, Northwestern Polytechnical University, Xi'an 710072, China*

[c]*Department of Mechanical Engineering, The Hong Kong Polytechnic University, Kowloon, Hong Kong*

[d]*Energy Systems Division, Argonne National Laboratory, Lemont, IL 60439, USA*

[e]*School of Energy and Power Engineering, Beihang University, Beijing, China*

ABSTRACT

H-atom abstraction by methoxy radical (CH3Ȯ) plays an important role in capturing the kinetics of reactions between gasoline components and alcohols. This study focuses on determining the reaction rates and thermodynamic properties of methoxy radical reactions with five gasoline fuel components: n-heptane, iso-octane, 1-hexene, cyclopentane and toluene. Electronic structure calculations were performed for all the stationary points with M06-2X/6-311++g(d,p) method. G3 composite method with atomization method is used for determining $\Delta_f H_0$ of all the closed shell and radical species, using which the necessary thermodynamic data of all the species was determined. Coupled cluster theory QCISD/cc-pVXZ (where X = D and T) and Møller–Plesset perturbation theory MP2/cc-pVXZ (where X = D, T and Q) were used to calculate single point energies. Subsequently, rate constants for all hydrogen atom abstraction channels have been performed using conventional transition state theory with unsymmetric tunneling corrections. A systematic comparison of rates for abstraction from different sites within the same species and same site from different species is done in order to get insights into this reaction class. The computed thermodynamic properties and rate constants were incorporated in to a recent gasoline mechanism to investigate the impact of the calculations performed in this work. A shift in

predicted NTC (negative temperature coefficient) behavior and significant reduction in model reactivity is observed upon incorporating the rates calculated herein.

1. INTRODUCTION

Chemical reaction kinetics govern fuel pyrolysis, oxidation and combustion in engines for different transportation systems, including on-road/off-road vehicles, transportation/combat aircrafts, space shuttles and rockets. Even small perturbations in reaction kinetics can significantly alter system efficiency, operating stability, and emissions. If chemical reaction kinetics can be predicted with high accuracy, manufacturers can build high-fidelity modeling tools to accelerate engineering design cycles for high efficiency and low emission engines and combustion strategies.

In combustion modeling, chemical reaction kinetics are specified via a chemical kinetic model. Historically, chemical kinetic models have been developed for single fuel components, then simply combined and, sometimes, with conservative adjustments to key kinetic parameters for complex fuel blends. When chemical kinetic models are built this way, the interactions between different fuel sub-chemistries are significantly overlooked. The lack of interactions between different fuel sub-chemistries has been recently identified by Cheng and co-workers [1,2] as a significant drawback of the existing chemical kinetic models for complex fuel blends, particularly for the blends of bio-fuels and petroleum-derived fuels. Through a series of studies, they demonstrated that a state-of-the-art chemical kinetic model [3] captured reasonably well the autoignition and preliminary heat release characteristics of neat alcohols (including ethanol, iso-propanol and iso-butanol) [4,5] and 'neat' gasoline [3,6], while showing significantly increased disagreement for their blends. Via a molecular tagging approach [1], Cheng and co-workers attributed this unique behavior to the inadequately defined interactions between alcohols and gasoline sub-chemistries in the model. They advocated to investigate several specific types of interactive chemical kinetic reactions, with one of which being the H-atom abstraction reactions from typical gasoline hydrocarbons by CH3Ȯ, a radical that can be considerably generated from both gasoline and alcohol oxidation.

Experimental and theoretical studies on H-atom abstraction reactions by CH3Ȯ radical are sparse. Gomez et al. [7] determined rate constants for the reactions of CH3Ȯ with cyclohexane, cyclohexene, and 1,4-cyclohexadiene. However, their experimental conditions spanned only low temperature (300-513 K) and their theoretical study did not employ accurate methods of quantum chemistry. Henon et al. [8] and Siai et al. [9] studied H- abstraction by CH3Ȯ from

formaldehyde. Zhang et al. [10] studied abstraction from acetaldehyde. However, H-atom abstraction reactions from typical gasoline hydrocarbons by CH3Ȯ are not present in literature. In this study, five gasoline fuel components namely n-heptane, iso-octane, 1-hexene, cyclopentane and toluene are investigated. The rates of all the H-abstraction by CH3Ȯ radical from all the possible sites of these five fuel components are determined. The thermochemistry of all the reactants and products involved these reactions is also computed in this study. Finally, the impacts of these reaction rates and thermochemistry of the participating species on the performance of a state-of-the-art gasoline/ethanol chemistry model [3] are investigated.

2. Methods and Procedure

2.1 Hydrocarbons

To study the H-atom abstraction reaction by CH3O, five hydrocarbons are considered, which are n-heptane, iso-octane, 1-hexene, cyclopentane and toluene. These hydrocarbons represent the most commonly used constituents for gasoline surrogate formulation, with each belonging to a unique hydrocarbon family, i.e., n-paraffin, iso-paraffin, olefin, naphthene and aromatic, respectively. The rate parameters for the H-atom abstraction reaction by CH3O from these fuel molecules can also provide a reliable baseline to estimate the rate parameters for other similar reactions by analogy.

2.2 Ab initio calculation

Electronic structure calculations of all the fuel species, their radicals and corresponding transition states for the reactions considered are first performed. The geometry, vibrational frequencies, and SPE of the species and transition states are necessary to calculate the kinetic data of the species and reactions. The geometry optimization is performed starting from a guess geometry and is varied until a successful optimization. The conformational space of this optimized structure of each species was screened to find the lowest potential energy conformer. The optimized geometry of the lowest energy conformer is then used for frequency and SPE calculations. The geometry optimization and frequency calculations are performed with M062X [11] method with 6-311++g(d,p) [12] basis set. SPE calculations using different methods are computed for calculating thermodynamic and kinetic data. Further, relaxed potential energy

scans in 10 degrees increments were performed for the dihedral angles, using the consistent method M062X/6-311++g(d,p), in order to obtain reduced moments of inertia for the hindered internal rotations that were fitted to truncated Fourier series. Those dihedral scans were used to account for the effects of torsional anharmonicity associated to the lower-frequency modes by using the hindered rotor approximation.

2.2.1 Thermodynamic data:

The standard practice to maintain thermodynamic consistency within a chemical kinetic mechanism is to provide the rate coefficient of a given reaction for the forward direction, and then compute those for the reverse direction by using the former ones and the equilibrium constants that are obtained from thermochemistry. This makes thermochemistry integral part of kinetic data of reactions in a mechanism. Thermodynamic data of species in the considered reactions is computed using statistical thermodynamics, i.e. the enthalpies of formation and entropies at 298.15 K as well as the temperature-dependent heat capacities. The vibrational frequencies and dihedral scans of the optimized geometries, together with the enthalpies of formation at 0 K ($\Delta_f H_0$), were used as input to the MultiWell program suit [13] to compute thermodynamic data using statistical thermodynamics. The enthalpies of formation at 0 K ($\Delta_f H_0$) of species are obtained from their Zero Kelvin Energy (ZKE) calculated using G3 composite method [14], in conjunction with atomization method. G3 is a composite method consisting of series of calculations and averaging over multiple methods. It has been shown to produce thermodynamic property values closer to benchmark methods []. The atomization method to obtain $\Delta_f H_0$ from ZKE, considers a molecule to be formed from its constituent atoms, as shown in Equation 1. The theoretical atomization energy at 0 K (TAE_0) is therefore calculated for the species C_xH_y using Equation 2, where H_0 is the ZKE calculated using G3 method. Finally, the enthalpy of formation of CxHy ($\Delta_f H_0$) is calculated from TAE_0 and the standard formation enthalpies of the component atoms in their gaseous state, as shown in Equation 3. The reference standard formation enthalpies of the component atoms were taken from the ATcT tables [15] as shown in Table S1.

$$x\mathrm{C} + y\mathrm{H} \rightarrow \mathrm{C}_x\mathrm{H}_y \quad \ldots\ldots\ldots\ldots (1)$$

$$\mathrm{TAE}_0 = x\, H_0(\mathrm{C}) + y\, H_0(\mathrm{H}) - H_0(\mathrm{C}_x\mathrm{H}_y) \quad \ldots (2)$$

$$\Delta_f H_0(\mathrm{C}_x\mathrm{H}_y) = x\, \Delta_f H_0(\mathrm{C}) + y\, \Delta_f H_0(\mathrm{H}) - \mathrm{TAE}_0 \quad ..(3)$$

2.2.2 Kinetic data:

The rate constants of considered reactions were computed using canonical transition state theory (TST). The electronic single-point energies (SPEs) required for TST are calculated using coupled cluster theory [16] QCISD/cc-pVXZ (where X = D and T) and Møller–Plesset perturbation theory [17] MP2/cc-pVXZ (where X = D, T and Q). Equation 4 is used for conducting the complete basis set (CBS) extrapolation [] of SPEs generated using aforthmentioned methods.

$$E_{QCISD/cc\text{-}pVTZ} + (E_{QCISD/cc\text{-}pVTZ} - E_{QCISD/cc\text{-}pVDZ}) \times 3^4/(4^4 - 3^4) + E_{MP2/cc\text{-}pVQZ} + (E_{MP2/cc\text{-}pVQZ} - E_{MP2/cc\text{-}pVTZ}) \times 4^4/(5^4 - 4^4) - E_{MP2/cc\text{-}pVTZ} - (E_{MP2/cc\text{-}pVTZ} - E_{MP2/cc\text{-}pVDZ}) \times 3^4/(4^4 - 3^4) \quad \ldots\ldots\ldots\ldots(4)$$

$$k = A\, T^n \exp(-E/RT) \quad \ldots\ldots.(5)$$

The calculated rate coefficients were fitted to a modified Arrhenius expression as a function of temperature, shown in equation 5. A is the frequency factor, T is the temperature in Kelvin, n is the temperature exponent at 1 K, and E is related to the activation energy (by Ea = E + nRT).

3. RESULTS AND DISCUSSION

In total, 16 abstraction reactions were systematically studied in this work, and they are 1, 1, 6, 4 and 4 reactions for cyclopentane, toluene, 1-hexene, n-heptane and iso-octane respectively. Figure 1 labels the different abstraction channels in 1-hexene, n-heptane and iso-octane molecules, and in the following paragraph, the radical products of these abstraction reactions will be named as C_6H_{11}-X, C_7H_{15}-Y, C_8H_{17}-Z, where X, Y and Z corresponds to the channel number shown in the Figure 1.

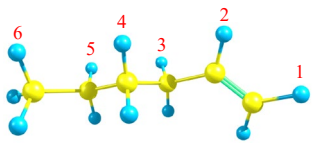

(1) 1-Hexene

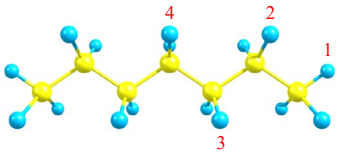

(2) n-Heptane

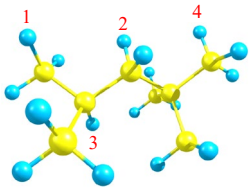

(3) iso-Octane

Figure 1 Abstraction channels in 1-hexene, n-heptane and iso-octane molecules

3.1 PES and barrier heights comparison:

The potential energy surface (PES) of all 16 reactions calculated in this study were generated simultaneously. Here, C_6H_{12}-1 + CH3Ȯ ↔ C_6H_{11}-3+ CH3OH reaction was selected as a representative, the PES of this reaction is shown in Figure 2. The reactants 1-hexene (C_6H_{12}-1) and methoxy radical (CH3Ȯ) undergo a 3.51 kcal/mol barrier to form an allylic radical (C_6H_{11}-3) plus methanol (CH3OH), and the exothermicity of this reaction is 20 kcal/mol. The barrier height of this reaction is found to be the lowest among all reactions, this reflects to the weakness of secondary allylic C-H bond.

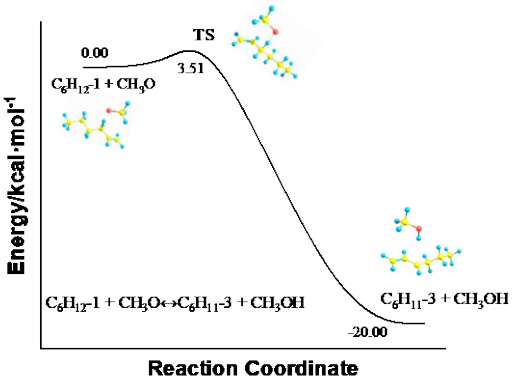

Figure 2 PES of C_6H_{12}-1 + CH3Ȯ ↔ C_6H_{11}-3+ CH3OH reaction

Table 1 compares the forward and reverse barrier heights of all X + CH3Ȯ reactions calculated by both Gaussian [18] and Orca [19]. Reaction C_6H_{12}-1 + CH3Ȯ ↔ C_6H_{11}-1+ CH3OH and C_6H_{12}-1 + CH3Ȯ ↔ C_6H_{11}-2+ CH3OH are vinylic and secondary vinylic H-atoms abstraction from 1-hexene, the strong vinylic C-H bond leads to a high forward barrier height, and both reactions are endothermic. Apart from these two reactions, all other reactions exhibit high exothermicity; forward barrier heights of the other 14 reactions are lower than 9 kcal/mol, while reverse barrier heights are higher than 11 kcal/mol.

When comparing barrier heights of different abstraction channels, in 1-hexene molecule, barrier height order from low to high is secondary allylic, secondary, primary, secondary vinylic and vinylic channel, and the difference between them are about 2-3 kcal/mol. In n-heptane and iso-octane molecules, barrier heights of abstraction tertiary H are lower than that from secondary H which is lower than that from primary site.

Comparing with the calculations from the companion study (please add reference here) where the H-atom abstraction reactions from the same fuel molecules but by CH3O2 were determined following the same computational methods, it is seen that the barrier heights with CH3O (c.f. Table 1 for 1-hexene calculations) at different H sites follow similar trends with those calculated for CH3O2. For instance, the barrier height at the allylic site is the smallest and that at the vinylic site is the greatest, and the barrier height always follow the order of primary H > secondary H > tertiary H (c.f. Table 1 for iso-octane calculations).

Table 1 Barrier heights comparison of all X + CH3Ȯ reactions calculated by Gaussian and Orca (Unit: kcal/mol)

Reactions	Gaussian		Orca	
	Forward	Reverse	Forward	Reverse
Cyclopentane + CH3Ȯ				
CPT + CH3Ȯ ↔ CYC_5H_9+ CH3OH	5.18	14.13	4.47	14.25
Toluene + CH3Ȯ				
$C_6H_5CH_3$ + CH3Ȯ ↔ $C_6H_5CH_2$+ CH3OH	6.32	19.61	5.50	19.63
n-Hexene + CH3Ȯ				
C_6H_{12}-1 + CH3Ȯ ↔ C_6H_{11}-1+ CH3OH	11.71	5.46	11.03	5.80
C_6H_{12}-1 + CH3Ȯ ↔ C_6H_{11}-2+ CH3OH	9.31	6.47	8.52	6.64
C_6H_{12}-1 + CH3Ȯ ↔ C_6H_{11}-3+ CH3OH	3.51	23.51	2.71	23.70

C_6H_{12}-1 + CH3Ȯ ↔ C_6H_{11}-4+ CH3OH	5.38	11.45	4.67	11.74
C_6H_{12}-1 + CH3Ȯ ↔ C_6H_{11}-5+ CH3OH	5.64	12.30	4.99	12.59
C_6H_{12}-1 + CH3Ȯ ↔ C_6H_{11}-6+ CH3OH	8.63	12.37	7.88	12.72
n-Heptane + CH3Ȯ				
C_7H_{16} + CH3Ȯ ↔ C_7H_{15}-1+ CH3OH	8.46	12.42	7.69	12.37
C_7H_{16} + CH3Ȯ ↔ C_7H_{15}-2+ CH3OH	5.54	12.22	4.88	12.55
C_7H_{16} + CH3Ȯ ↔ C_7H_{15}-3+ CH3OH	5.09	11.45	4.57	11.92
C_7H_{16} + CH3Ȯ ↔ C_7H_{15}-4+ CH3OH	5.04	11.49	4.34	11.76
Iso-Octane + CH3Ȯ				
C_8H_{18} + CH3Ȯ ↔ C_6H_{11}-1+ CH3OH	7.76	11.98	7.07	12.31
C_8H_{18} + CH3Ȯ ↔ C_6H_{11}-2+ CH3OH	4.65	12.53	3.67	12.55
C_8H_{18} + CH3Ȯ ↔ C_6H_{11}-3+ CH3OH	3.95	14.77	2.97	14.55
C_8H_{18} + CH3Ȯ ↔ C_6H_{11}-4+ CH3OH	8.05	12.29	6.79	16.14

When comparing Gaussian and Orca solver, two solvers give quite consistent results. Overall, the difference for both forward and reverse barriers are within 1 kcal/mol, with the averaged difference being well below 1 kcal/mol. Figure 3 shows the Evans–Polanyi relationship for all the abstraction reactions studied in this work. The activation energy is indeed in linear relationship with the heat of reaction, except the allylic and vinylic sites. The linear relationship is found to be $E_a = 0.63\Delta H_f^o + 10.22$, for the CH3Ȯ abstraction.

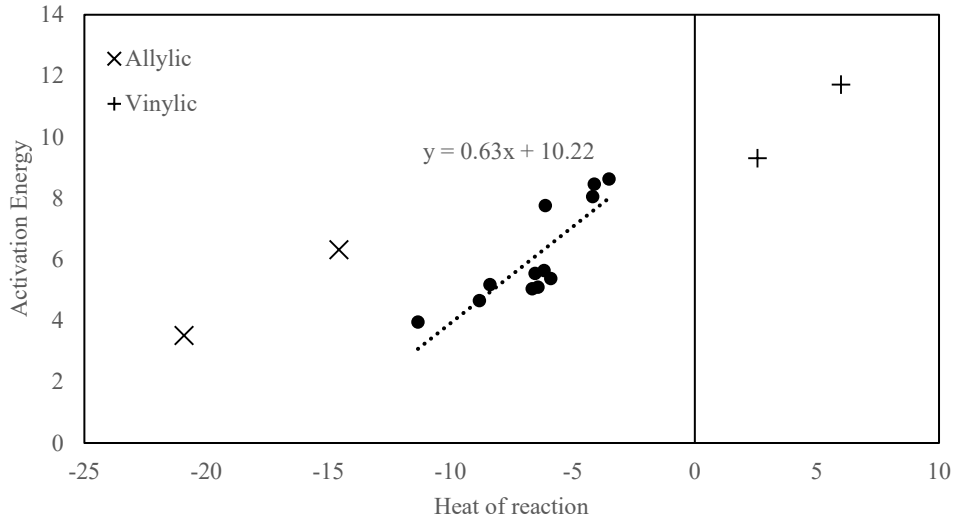

Figure 3 Evans–Polanyi relationship between activation energy and heat of reactions for all the abstraction reactions studied in this work

Recently, Gomez et al. [7] performed both experimental measurement and theoretical calculations for the barrier heights and rate constants of the reactions of CH3Ȯ with cyclohexane (CHX). Given the similar structure between cyclopentane (CPT) and cyclohexane, the barrier height of CH3Ȯ reacting with the two molecules were compared in Table 2. The barrier height obtained by Gaussian agrees well with the experimental value from Gomez et al., wherein the difference is 0.68 kcal/mol. Notably, the rate constant comparison will also be made in the next section.

Table 2 Barrier height comparison between CPT + CH3Ȯ (current study) and CHX + CH3Ȯ (Gomez et al. [7]) (Unit: kcal/mol)

Source	Method or Solver	Barrier height
Current study	Gaussian	5.18
	Orca	4.47
Gomez et al.	Experiment	5.86
	UMP2	4.40
	UMP4(SDQ)	8.48
	PMP2	1.39
	HF-DFT (B3LYP)	2.49
	CASPT2	4.40

3.2 Rate constants comparison:

Figure 4 compares the rates between CPT + CH3Ȯ (current study) and CHX + CH3Ȯ (Gomez et al.), black solid and dash lines represent the rates calculated by Gaussian and Orca solvers respectively, while, solid symbols and other lines correspond to the experimental data and theoretical results generated using different levels of theory from Gomez et al. It is found that the rate carried out by Orca solver shows excellent agreement with the experimental data, while Gaussian solver slightly under predicts the rate by about a factor of 2. Ultimately, CPT + CH3Ȯ and CHX + CH3Ȯ are different reactions, so such comparison does not signify the accuracy of our calculation results. However, it shows the order of rate constant when abstracting an H-atom from a cyclic hydrocarbon by CH3Ȯ radical.

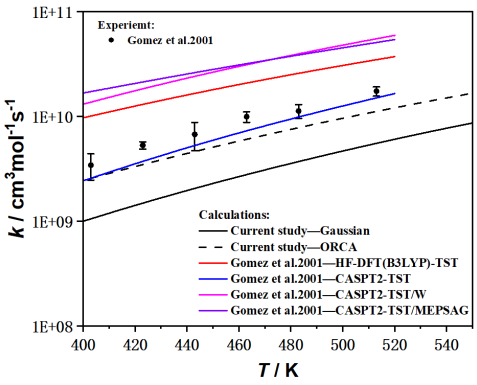

Figure 4 Rate constant comparison between CPT + CH3Ȯ (current study) and CHX + CH3Ȯ (Gomez et al.)

All the rate constants computed using Gaussian and Orca are plotted in supplementary material 1 and are given in Arrhenius format in supplementary material 2. Moreover, all calculated rate constants have also been comprehensively compared in two dimensions: (1) Rate of abstracting different H-atoms in a same molecule; (2) Rate of abstracting same type of H-atoms in different molecules. Note that these rate constants comparisons are for abstraction on a per H-atom basis, and all input and output results have been summarized in the Supplementary Material 3 and 4. Figure 5 shows the rate constant comparison of abstracting different H-atoms in a same molecule. In each figure, H-atoms circled with different colors corresponds to rate constants of different reactions respectively.

For n-heptane + CH3Ȯ reaction series, given the symmetric structure of n-heptane molecule, the rate of abstracting one primary H-atom and three secondary H-atom was compared. It can be seen that secondary H-atom abstraction show quite high consistency, with the largest discrepancy appeared at 2000 K, the rate of abstracting NO.2 H-atom is a factor of 1.67 higher than that of NO.4 H-atom. While, below 1100 K, the rate of abstracting primary H-atom is found to be slower than abstracting any secondary H-atoms in the molecule.

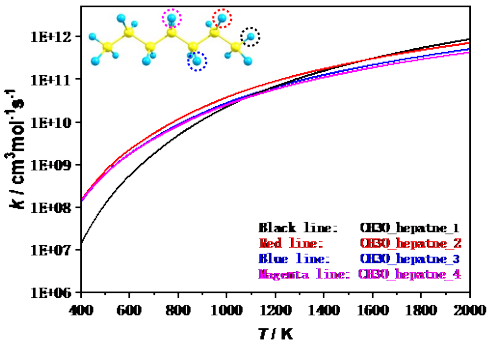

(a) n-Heptane + CH3Ȯ

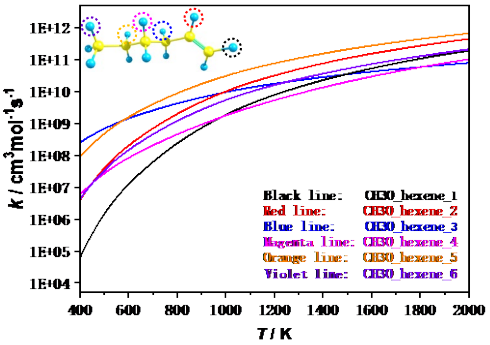

(b) 1-Hexene + CH3Ȯ

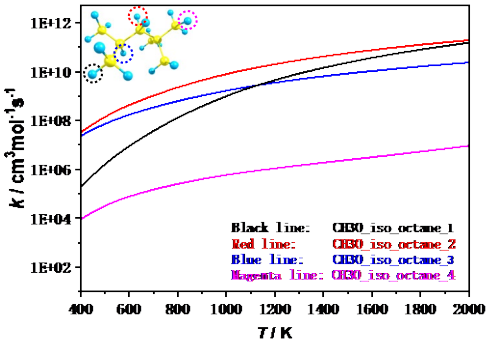

(c) iso-Octane + CH3Ȯ

Figure 5 Rate constant comparison of abstracting different H-atoms on per H-atom basis in (a) n-Heptane, (b) 1-Hexene and (c) iso-Octane molecules

For 1-hexene + CH3Ȯ reaction series, the rate of abstracting vinylic, secondary vinylic, secondary allylic, secondary and primary H-atom were systematically compared. Below 1000 K,

abstracting a vinylic H-atom exhibits the lowest rate among all hydrogen types, above 600 K, abstracting the NO.5 secondary H-atom shows the fastest rate. While, below 600 K, the rate of abstracting the secondary allylic H-atom dominate, and it exhibits the least temperature dependency. In other words, with the increasing temperature, the aforementioned reaction increases more gently than other reactions.

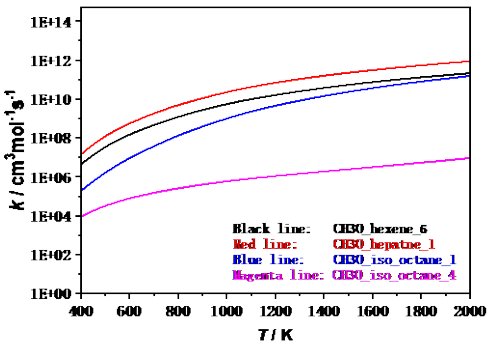

(a) Primary H-atom abstraction

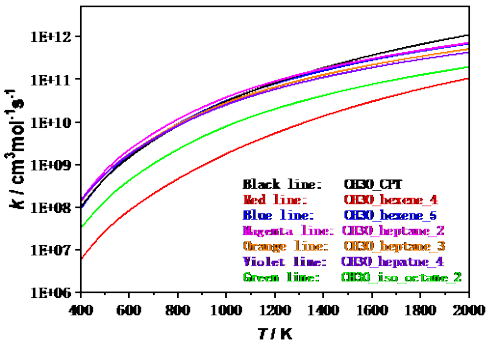

(b) Secondary H-atom abstraction

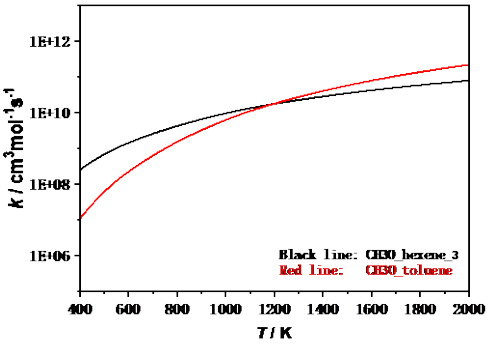

(c) Allylic H-atom abstraction

Figure 6 Rate constant comparison of abstracting same type of H-atoms on per H-atom basis in different molecules

For iso-Octane + CH3Ȯ reaction series, the rate of abstracting primary, secondary and tertiary H-atom were compared. It is found that the rate of abstracting NO.1 primary, NO.2 secondary and NO.3 tertiary H-atom abstraction is quite close from 1000 – 2000 K regime, whereas, NO.4 primary H-atom abstraction is significantly slower, we believe a further investigation is required for this reaction.

Figure 6 shows the rate constant comparison of abstracting same type of H-atoms in different molecules. For primary H-atom abstraction, apart from the NO.4 primary H-atom abstraction from iso-octane molecule mentioned above, the rates of abstracting the primary H-atom from 1-hexene, n-heptane and iso-octane are close to each other. For secondary H-atom abstraction, the rates of abstraction from cyclopentane, n-heptane and NO.5 H-atom are identical. For allylic H-atom abstraction, above 1200 K, the rate of abstracting secondary allylic H-atom from 1-hexene is faster than primary allylic H-atom from toluene, and the situation turns into the opposite when temperature is below 1200 K.

3.3 Thermochemistry:

In this study, the thermochemistry of all reactants and products were also carried out by ab initio calculation combined with statistic thermodynamic theory. The 298 K enthalpy of formation, entropy and temperature dependent heat capacity have been summarized in Table S2 of Supplementary Material 1, and the NASA polynomial format data has been collected in Supplementary Material 2. In addition, a comparison of the standard enthalpy values from this work with that of the ATcT values is provided for those species with the data in ATcT tables [] is shown in Table S2. Also provided in the Table S1 are the comparison of the thermodynamic properties calculated in this work with that of Goldsmith et al. [] for the methanol and its radical. As can be seen, for both cases, the values are in good agreement.

3.4 Effect on global chemical properties:

To evaluate the impact of the CH3O reactions and the thermochemistry for the participating species, the computed kinetic and thermochemical data are incorporated into the latest gasoline/ethanol chemical kinetic model proposed by Cheng et al. [3]. The updated model is then used to model a set of autoignition experiments acquired in a rapid compression machine (RCM) for different blends of FGF-LLNL (a five-component gasoline surrogate containing n-heptane, iso-octane, 1-hexene, cyclopentane and toluene) and ethanol at stoichiometry of 1.0, ~15% O2, Pc = 40 bar and Tc = 700–1000 K [3]. It should be noted that this is the same dataset used in [1], wherein the original chemistry model displayed reasonable agreement with the experiments for "neat" FGF-LLNL and neat ethanol, while showing significant discrepancies for their blends. Five different blends containing 0%, 10%, 20%, 30% and 100% ethanol by volume are considered, which are referred to as E0, E10, E20, E30 and E100, respectively. Simulations of the RCM experiments are competed using fast chemical kinetic solver ZeroRK, with volume histories derived from non-reactive tests to account for compression and heat loss effects. The simulation results using the updated model, along with the experimental measurements and the simulation results using the original model taken from [3,4], are illustrated in Fig. 6.

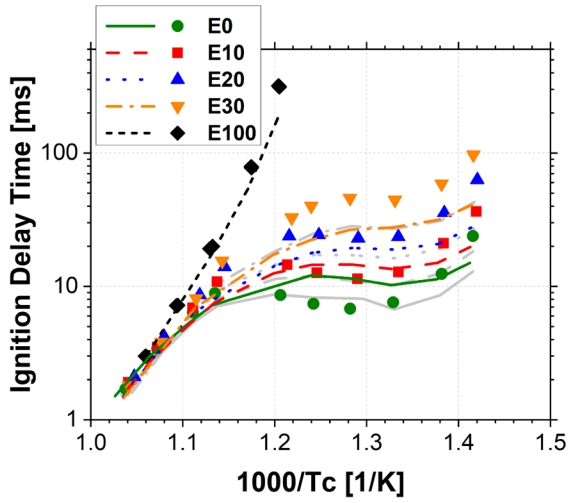

Figure 7 Simulated (lines) and measured (symbols) ignition delay times for FGF-LLNL/E0–E100 at phi = 1.0, ~15% O2, Pc = 40 bar and Tc = 700–1000 K. Experiments for neat ethanol and FGF-LLNL/E0–E30 are taken from [4] and [3], respectively. Simulations are conducted using the gasoline surrogate model proposed in [3]. Color lines are the simulation results using

the model with the updated kinetic and thermochemical data, and grey lines with the corresponding line types are the simulation results using the original model. .

Immediately seen in Fig. 6 is the strong impact of these reactions on model performance, where incorporating the computed kinetic and thermochemical data from this study into the original model leads to shifts in predicted NTC (negative temperature coefficient) behavior and significant reduction in model reactivity. The suppression of model reactivity is most obvious within the NTC regime, less pronounced within the low-temperature regime, and negligible within the intermediate to high temperature regimes. Also seen in Fig. 6 is that greater reduction in model reactivity is observed at lower levels of ethanol blending (e.g., difference between the updated and original models is the greatest for E0, less significant for E10 and E20, and negligible for E30), indicating that CH3Ȯ radicals are mostly produced from FGF-LLNL. This trend is different from the trend observed in the companion study of this study [20], where H-atom abstractions from gasoline fuels by CH3ȮO are found to be more influential at higher ethanol concentrations. This, however, does not mean that H-atom abstractions by CH3Ȯ do not contribute to gasoline/ethanol interactions, since CH3Ȯ generated in FGF-LLNL oxidation can participate in H-atom abstraction from ethanol. This type of reaction is not covered in this study. Quantitative comparisons between Fig. 7 in this study and Fig. 6 in the companion study (where the impact of CH3O2 reactions on model performance was characterized) indicate that CH3O reactions are more prominent for "neat" FGF-LLNL and at higher temperatures within the NTC regime, while the CH3O2 reactions are more impactful for FGF-LLNL/ethanol blends and at relatively lower temperatures. The relative higher impact of CH3O2 reactions than CH3O reactions at lower temperatures is somewhat expected since RO2 chemistry are more dominant than RO radicals at lower temperatures. CH3O reactions being the most impactful on "neat" FGF-LLNL reactivity implies that CH3O is mostly produced from the FGF-LLNL components rather than ethanol, which is supported by the findings in (please insert ref [1] here)

It is important to recognize that this study does not aim to provide an immediate solution to fix the model adequately, but rather to highlight the importance of H-atom abstractions by CH3Ȯ, which has been seriously overlooked in the past. The changes implemented in the updated model do not lead to satisfactory agreement with the experiments, indicating that there exist other contributors to the unique interactions between gasoline fuels and ethanol that still requires

further investigation. These investigations should be carried out based on the findings from this study and its companion study [20].

3.5 Specific effects of the computed data:

In this section, further investigation on the specific effect of each of the new data generated from this (i.e., for the CH3O reaction system) and the companion study [20] (i.e., for the CH3O2 reaction system) is done. Figure 7 shows the effect of adding each of the computed data separately and combined on the original model [3]. First the effect of adding the computed kinetic and thermodynamic data (including abstraction by both $CH3\dot{O}$ and $CH3\dot{O}_2$) for each of the five components cyclopentane, toluene, 1-hexene, n-heptane and iso-octane is done. Overall, incorporating each of these separately has all reduced reactivity in low and intermediate temperature, except for ~800 K for E0 for which the reactivity seems to be increased. Further, adding all the data collectively for all the five components for $CH3\dot{O}$ and $CH3\dot{O}_2$ is compared with original model. Both these additions have the most impact relative to adding any individual component data and $CH3\dot{O}_2$ has marginally greater effect. Overall, the majority of the effect is observed for temperatures at NTC region around ~850 K and minor effect is observed for the other temperatures.

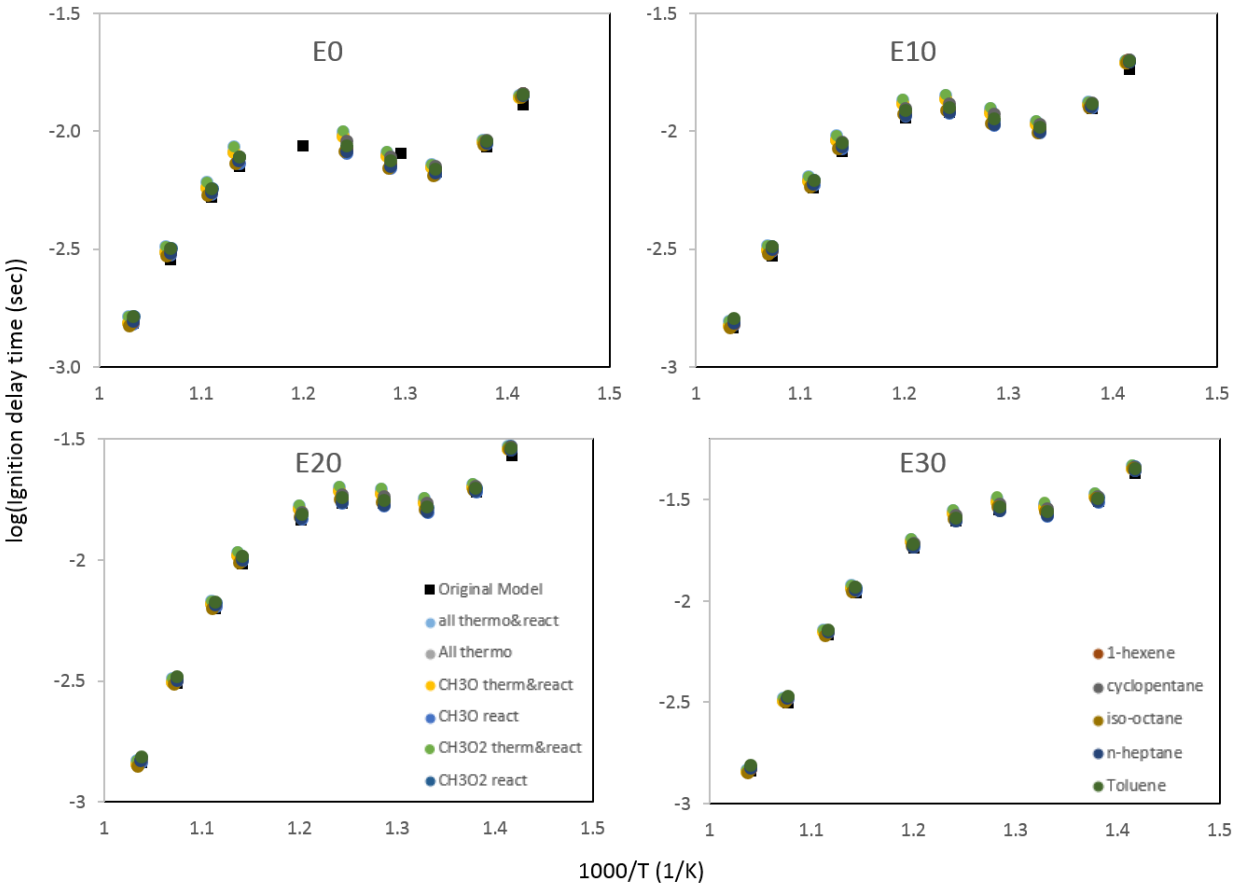

Figure 8 Effect of computed rate constants and thermodynamic data of the original model on ignition delay times at phi = 1.0, ~15% O2, Pc = 40 bar and Tc = 700–1000 K for FGF-LLNL/E0–E30 blends. Labels indicate the respective kinetic and thermodynamic data that was updated for that case.

In addition, a comparison of sensitivities of the reactions for which rate calculations are performed is done for the same conditions used in the former comparison at two representative temperatures of 750 and 900 K. Figure 8 shows the comparison of sensitivities for the different abstraction reactions by $CH3\dot{O}$ and $CH3\dot{O}_2$ that are studied in this and companion studies [20]. Figure 8 only shows the comparison for the maximum positive sensitivity at 750 K; however the trend is same for all the other cases of negative and 900 K cases (shown in the supplementary material 1). It is found that there is a significant difference in the sensitivities with the updated rate values. The maximum differences are observed for iso-octane abstractions. Note that some of the reactions studied are not presented in Figure 8 due to their sensitivities being below

tolerance limit. Therefore, from the aforth two comparisons, it is clear that the computed rate constants have a considerable effect on the kinetic mechanism and further investigations are needed to fully understand the discrepancies between the kinetic model and experiments that are still present.

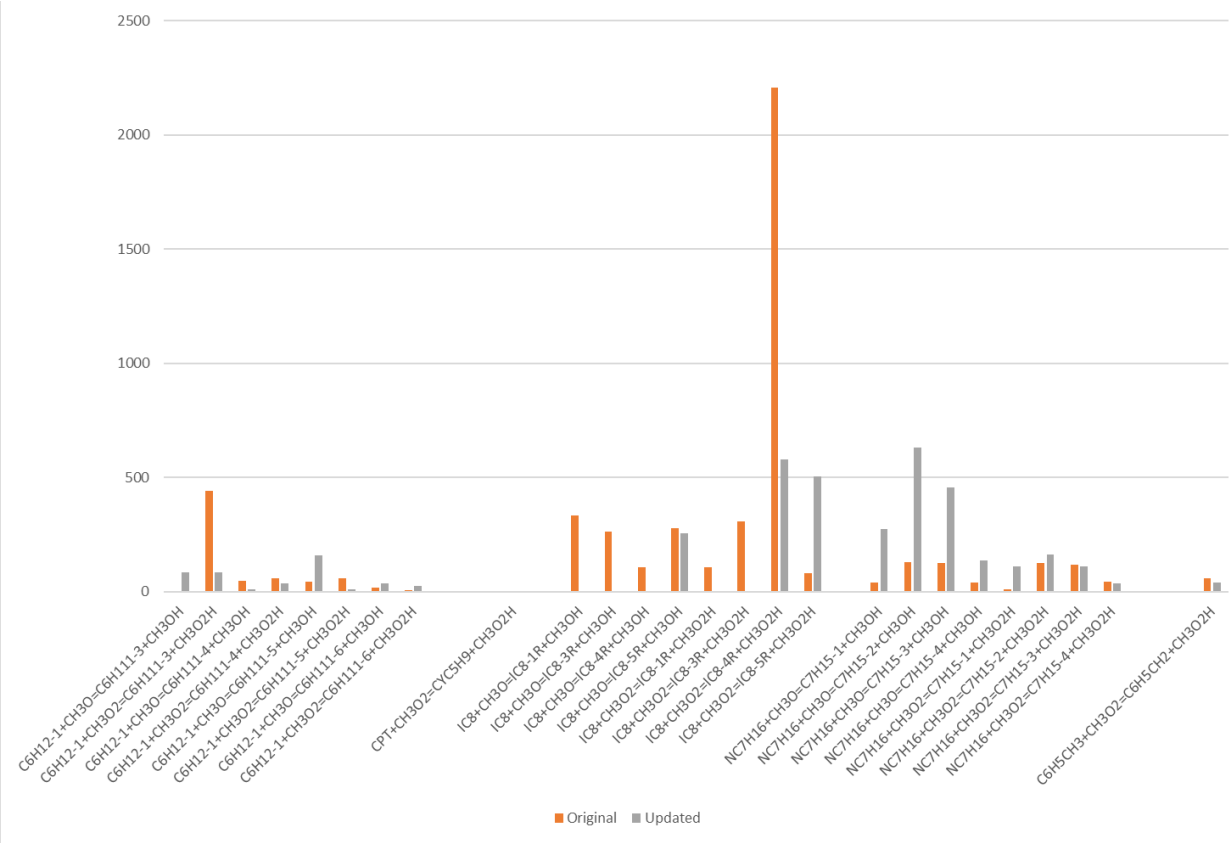

Figure 9 Comparisons of maximum sensitivities between original and updated models of the rates calculated in this study. The y-axis shows the Jacobean sensitivities values of ignition delay times at 750 K.

4. CONCLUSIONS

Hydrogen atom abstraction by CH3Ȯ radical from the five components of FGF-LLNL: cyclopentane, toluene, 1-hexene, n-heptane and iso-octane, is investigated in this work. Geometry optimizations and frequency calculations of all of the species involved have been calculated at M06-2X/6-311++G(d,p) level of theory. The electronic SPEs are reported at

coupled cluster theory QCISD/cc-pVXZ (where X = D and T) and Møller–Plesset perturbation theory MP2/cc-pVXZ (where X = D, T and Q), using Gaussian 16 and ORCA. The energy barriers for all the 16 possible reaction channels were obtained. Temperature dependent rate constants were determined at temperatures ranging from 298.15 to 2000 K, using conventional transition state theory with unsymmetric tunneling corrections. It was found that both Gaussian 16 and ORCA gave consistent results, overall, the difference for both forward and reverse barriers are within 1 kcal/mol between the two solvers. Temperature-dependent thermochemical properties for all stable species were also calculated.

Overall, C6H12-1 + CH3Ȯ ↔ C6H11-3+ CH3OH reaction was found to have lowest barrier height among all reactions, due to the weakness of secondary allylic C-H bond and highest is found for reaction C6H12-1 + CH3Ȯ ↔ C6H11-1+ CH3OH. A systematic analysis is also performed for comparing abstraction of different H-atoms in a same molecule, abstraction of same type of H-atoms in different molecules and comparing the barrier height effect on rate constant prediction. Computed kinetic and thermochemical data are incorporated into the latest gasoline/ethanol chemical kinetic model proposed by Cheng et al. [3]. A considerable impact of these reactions is observed on model performance, where incorporating calculations from this study into the original model leads to shifts in predicted NTC (negative temperature coefficient) behavior and significant reduction in model reactivity. It is also observed that changes implemented in the updated model do not lead to satisfactory agreement with the experiments, indicating that there exist other contributors to the unique interactions between gasoline fuels and ethanol that still requires further investigation.

5. ACKNOWLEDGEMENTS

The authors acknowledge the funding support: Fundamental Research of Free Orientation from Central Government (2021Szvup113). The work at KAUST was supported by the Supercomputing Lab and Clean Combustion Research Center. The work at ANL was supported by the U.S. Department of Energy, Argonne National Laboratory LDRD program No. 2021-0344, and the Laboratory Computing Resource Center at Argonne. The work at The Hong Kong Polytechnic University was supported by the Research Grant Council (PolyU) under P0039589. The authors also acknowledge Dr. Russell Whitesides from Lawrence Livermore National Laboratory for performing the ZeroRK simulations.

REFERENCES

[1] S. Cheng, S.S. Goldsborough, C. Saggese, S.W. Wagnon, W.J. Pitz, New insights into fuel blending effects: Intermolecular chemical kinetic interactions affecting autoignition times and intermediate-temperature heat release, Combust. Flame 233 (2021) 111559.

[2] S. Cheng, S.S. Goldsborough, S.W. Wagnon, W.J. Pitz, Probing intermediate temperature heat release in autoignition of C3-C4 iso-alcohol/gasoline blends, Combust. Flame 233 (2021) 111602.

[3] S. Cheng, C. Saggese, D. Kang, S.S. Goldsborough, S.W. Wagnon, G. Kukkadapu, et al., Autoignition and preliminary heat release of gasoline surrogates and their blends with ethanol at engine-relevant conditions: Experiments and comprehensive kinetic modeling, Combust. Flame 228 (2021) 57–77.

[4] S. Cheng, D. Kang, S.S. Goldsborough, C. Saggese, S.W. Wagnon, W.J. Pitz, Experimental and modeling study of C2--C4 alcohol autoignition at intermediate temperature conditions, Proc. Combust. Inst. 38 (1) (2021) 709–17.

[5] S.S. Goldsborough, S. Cheng, D. Kang, C. Saggese, S.W. Wagnon, W.J. Pitz, Effects of isoalcohol blending with gasoline on autoignition behavior in a rapid compression machine: Isopropanol and isobutanol, Proc. Combust. Inst. 38 (4) (2021) 5655–64.

[6] S. Cheng, D. Kang, A. Fridlyand, S.S. Goldsborough, C. Saggese, S. Wagnon, et al., Autoignition behavior of gasoline/ethanol blends at engine-relevant conditions, Combust. Flame 216 (2020) 369–84.

[7] N. Gomez, E. Hénon, F. Bohr, P. Devolder, Rate Constants for the Reactions of CH3Ȯ with Cyclohexane, Cyclohexene, and 1,4-Cyclohexadiene: Variable Temperature Experiments and Theoretical Comparison of Addition and H-Abstraction Channels, J. Phys. Chem. A 105 (50) (2001) 11204–11.

[8] E. Henon, F. Bohr, Theoretical study of the H-abstraction reaction of the CH3Ȯ radical with formaldehyde, Chem. Phys. Lett. 342 (5) (2001) 659–66.

[9] A. Siaï, I. Oueslati, B. Kerkeni, Quantum chemistry and dynamics of the abstraction reaction of H atoms from formaldehyde, Chem. Phys. 474 (2016) 44–51.

[10] Y. Zhang, R. Song, Y. Sun, R. Wang, Theoretical study on the gas-phase reaction of acetaldehyde with methoxy radical, Struct. Chem. 30 (2018) 127–35.

[11] Y. Zhao, D.G. Truhlar, The M06 suite of density functionals for main group thermochemistry, thermochemical kinetics, noncovalent interactions, excited states, and transition elements: two new functionals and systematic testing of four M06-class functionals and 12 other function, Theor. Chem. Acc. 120 (1) (2008) 215–41.

[12] R. Krishnan, J.S. Binkley, R. Seeger, J.A. Pople, Self-consistent molecular orbital methods. XX. A basis set for correlated wave functions, J. Chem. Phys. 72 (1) (1980) 650–4.

[13] J.R. Barker, Multiple-Well, multiple-path unimolecular reaction systems. I. MultiWell computer program suite, Int. J. Chem. Kinet. 33 (4) (2001) 232–45.

[14] L.A. Curtiss, K. Raghavachari, P.C. Redfern, V. Rassolov, J.A. Pople, Gaussian-3 (G3) theory for molecules containing first and second-row atoms, J. Chem. Phys. 109 (18) (1998) 7764–76.

[15] B. Ruscic, R.E. Pinzon, G. von Laszewski, D. Kodeboyina, A. Burcat, D. Leahy, et al., Active Thermochemical Tables: thermochemistry for the 21st century, J. Phys. Conf. Ser. 16 (2005) 561–70.

[16] K. Raghavachari, G.W. Trucks, J.A. Pople, M. Head-Gordon, A fifth-order perturbation comparison of electron correlation theories, Chem. Phys. Lett. 157 (6) (1989) 479–83.

[17] S. Grimme, Improved second-order Møller--Plesset perturbation theory by separate scaling of parallel-and antiparallel-spin pair correlation energies, J. Chem. Phys. 118 (20) (2003) 9095–102.

[18] M.J. Frisch, G.W. Trucks, H.B. Schlegel, G.E. Scuseria, M. a. Robb, J.R. Cheeseman, et al., G16_C01, 2016, p. Gaussian 16, Revision C.01, Gaussian, Inc., Wallin.

[19] F. Neese, Software update: the ORCA program system, version 4.0, WIREs Comput. Mol. Sci. 8 (1) (2018) e1327.

20] C. Yang, J. Chen, X. Zhu, S. Cheng, Y. Li, K. K. Yalamanchi, S. M. Sarathy et al., From electronic structure to model application of key reactions for gasoline/alcohol combustion, part I: hydrogen-atom abstractions by CH3ȮȮ radical, Proc. Combust. Inst., Under Review, 2022.